32ND INTERNATIONAL COSMIC RAY CONFERENCE, BEIJING 2011

Energy calibration of data recorded with the surface detectors of the Pierre Auger Observatory: an update

ROBERTO PESCE[1] FOR THE PIERRE AUGER COLLABORATION[2]
[1]*Università di Genova and INFN, Via Dodecaneso 33, 16146 Genova, Italy*
[2]*Observatorio Pierre Auger, Av. San Martin Norte 304, 5613 Malargüe, Argentina*
(Full author list: http://www.auger.org/archive/authors_2011_05.html)
auger_spokespersons@fnal.gov
DOI: 10.7529/ICRC2011/V02/1160

Abstract: The energy of the primary particles of air showers recorded using the water-Cherenkov detectors of the Pierre Auger Observatory is inferred from simultaneous measurements of showers with those detectors together with the fluorescence telescopes. The signal on the ground at 1000 m from the shower axis obtained using the water-Cherenkov detectors is related directly to the calorimetric energy measured with the telescopes. The energy assignment is therefore independent of air shower simulations except for the assumptions that must be made about the energy carried into the ground by neutrinos and muons. The correlation between the signal at the ground and the calorimetric energy is used to derive a calibration curve. Taking advantage of increased statistics with respect to previous publications we present an update and improvement of the method used to determine the energy scale. The systematic uncertainties of the calibration procedure are addressed.

Keywords: UHECR, energy spectrum, Pierre Auger Observatory, energy calibration.

1 Introduction

The Pierre Auger Observatory [1] is used to detect extensive air showers (EAS) with an array of over 1600 water-Cherenkov detectors, collectively called the Surface Detector Array (SD). The SD measures the lateral distribution of particles on ground with a duty cycle of almost 100% [2]. The SD is overlooked by the Fluorescence Detector (FD), which consists of 27 fluorescence telescopes at four locations on the periphery of the SD. The FD is only used on clear moonless nights and has a duty cycle of 13% [3]. The FD provides a nearly calorimetric energy measurement, since the fluorescence light is produced in proportion to the energy dissipation by a shower in the atmosphere [4, 5].

The signals recorded by the SD are converted into units of vertical-equivalent muons (VEM). One VEM is defined as the average of the signals produced in the 3 PMTs of a water-Cherenkov detector by a vertical muon that passes centrally through it. The EAS axis is obtained from the arrival time of the first particles in each detector station. The core and the lateral distribution function (LDF) are inferred from a global minimization, taking into account the SD station trigger threshold and the overflow of FADC counts in the detectors near the axis of the EAS. In general the energy of the primary particle is correlated with the signal at a fixed distance from the core of the EAS [6]. In this case, the signal at $1000\,\mathrm{m}$ from the axis, $S(1000)$, corrected for the attenuation in the atmosphere (see Section 2), is used as an energy estimator. At this distance, the fluctuations of the signal, due to an imperfect knowledge of the LDF, are minimized [7].

A measurement of the development profile of the air shower (deposited energy versus slant depth) is possible with EAS viewed with the FD in coincidence with the SD. The first step is the determination of the geometry of the axis of the EAS using directions and timing information from the FD pixels, coupled with the arrival time of the shower at the SD station with the highest signal. The procedure results in an arrival direction resolution of better than 1°. Next, the light collected in the cameras of FD is transformed into the energy deposited along the axis of the shower [8], by taking into account the fluorescence and Cherenkov light contributions and the attenuation of this light by scattering, including multiple scattering [9]. Care is taken to account for the lateral spread of light on the camera due to the emission of both fluorescence and Cherenkov light. The fluorescence light emission along the track of the EAS is converted into energy deposit by using the absolute fluorescence yield in air in the $337\,\mathrm{nm}$ band of (5.05 ± 0.71) photons$/\mathrm{MeV}$ of energy deposited [10]. This figure is for dry air at $293\,\mathrm{K}$ and $1013\,\mathrm{hPa}$: the wavelength, temperature, pressure and humidity dependence is accounted for using [11]. Due to the limited field of view of the FD, the longitudinal profile is not recorded in its entirety, so a fit with a Gaisser-Hillas function is employed to obtain the full profile. This energy deposit profile is in-

tegrated to yield the calorimetric energy, with a correction of about 9% added to take account of the energy carried by high energy muons and neutrinos. This non-detected energy, that is the *invisible energy*, is accounted for by correcting the calorimetric energy $E_{\rm cal}$, detected by the FD. The factor $f_{\rm inv}$ is determined from simulations to obtain the total shower energy $E_{\rm FD} = (1 + f_{\rm inv})\, E_{\rm cal}$. The invisible energy correction is based on the average for proton and iron showers simulated with the QGSJetII model [12] and amounts to about 9% at $10\,{\rm EeV}$ for a mixed primary composition [13]. The neutrino and muon production probabilities have energy dependencies due to the meson decay probabilities in the atmosphere so that $f_{\rm inv}$ falls from $\sim 10.5\%$ at $1\,{\rm EeV}$ to $\sim 8.5\%$ at $100\,{\rm EeV}$ [13]. The factor $f_{\rm inv}$ depends on the hadronic interaction assumptions and is also subject to shower-to-shower fluctuations [14]. The dependence of the energy scale on the hadronic interaction model is below 4%.

The sub-sample of EAS that are recorded by both the FD and the SD, called *golden hybrid events*, is used to relate the energy reconstructed with the FD, $E_{\rm FD}$, to $S(1000)$. The energy scale inferred from this data sample is applied to all showers detected by the SD array.

2 Data Analysis

A subset of high-quality golden hybrid events detected between 1 January 2004 and 30 September 2010 is used in this analysis, an update and an improvement with respect to the one presented in [15]. Golden hybrid events are those for which the reconstruction of an energy estimator can be derived independently from both the SD and FD data. In this work only events with reconstructed zenith angles less than 60° are used.

A fiducial cut is applied to events recorded by the SD to ensure adequate containment inside the array, and hence a reliable core reconstruction and estimate of $S(1000)$. The cut requires that six active stations surround the station with the highest signal [16]. The water-Cherenkov detector with the highest signal must be within $750\,{\rm m}$ of the shower axis [17]. The reduced χ^2 of the longitudinal profile fit to the Gaisser-Hillas function has to be less than 2.5. Furthermore the χ^2 of a linear fit to the longitudinal profile has to exceed the Gaisser-Hillas fit χ^2 by at least 4 [8]. The depth of shower maximum, $X_{\rm max}$, must be within the field of view of the telescopes and the fraction of the signal detected by the FD and attributed to Cherenkov light must be less than 50%. The uncertainties on $E_{\rm FD}$ and on $X_{\rm max}$ are required to be less than 20% and $40\,{\rm g/cm^2}$ respectively. The selection criteria include a measurement of the vertical aerosol optical depth profile (VAOD) made using laser shots generated by the central laser facility (CLF) [18] and observed by the fluorescence telescopes in the same hour of each selected hybrid event; the VAOD value must be smaller than 0.1. Furthermore the cloud fraction in the field of view, measured from the information provided by the LIDAR systems of the observatory [18], is required to be less than 25%. The limited field of view of the FD and the requirement to observe the EAS maximum may introduce a dependency in the event selection on the primary mass. To avoid this effect, a fiducial cut on the slant depth range observed by the telescopes is performed [19], ensuring that the field of view is large enough to observe all plausible values of $X_{\rm max}$. This cut is introduced for the first time in this analysis, taking advantage of the increased statistics of data. The effect of this fiducial cut is to reject about 22% of events above $3\,{\rm EeV}$ and 4% above $10\,{\rm EeV}$. As explained in Section 3, the application of this cut does not change the results of the energy calibration significantly. Applying these cuts, a set of 839 golden hybrid events with energy $E_{\rm FD} \geq 3\,{\rm EeV}$ (where the SD trigger is fully efficient [16]) is selected.

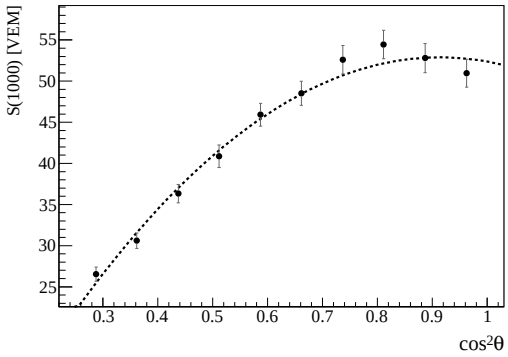

Figure 1: Attenuation curve, $\mathrm{CIC}(\theta)$ fitted with a second degree polynomial in $x = \cos^2\theta - \cos^2\bar{\theta}$.

For a given energy, the value of $S(1000)$ decreases with the zenith angle, θ, due to the attenuation of the shower particles and geometrical effects. Assuming an isotropic flux of primary cosmic rays, we extract the shape of the attenuation curve from the data using the constant intensity cut method [20]. The attenuation curve has been fitted with a second degree polynomial in $x = \cos^2\theta - \cos^2\bar{\theta}$: $\mathrm{CIC}(\theta) = 1 + a\,x + b\,x^2$, where $a = (0.87 \pm 0.04)$ and $b = (-1.49 \pm 0.20)$. The attenuation curve is shown in Fig. 1. The average angle, $\bar{\theta} \simeq 38^\circ$, is taken as a reference to convert $S(1000)$ to $S_{38} \equiv S(1000)/\mathrm{CIC}(\theta)$. S_{38} may be regarded as the signal $S(1000)$ the shower would have produced if it had arrived at $\theta = 38^\circ$. The values of the parameters a, b are deduced for $S_{38} = 47\,{\rm VEM}$, that corresponds to an energy of about $9\,{\rm EeV}$ (see Section 3). The relative difference of the $\mathrm{CIC}(\theta)$ with respect to the previous analysis [15] is about $(-4 \pm 4)\%$ for $\theta = 0^\circ$ and $(-4 \pm 9)\%$ for $\theta = 60^\circ$, i.e. the values of S_{38} are reduced by about 4%.

The reconstruction accuracy $\sigma_{S(1000)}$ of $S(1000)$ is composed of three contributions: a statistical uncertainty due to the finite number of particles intercepted by a given SD station and the limited dynamic range of the signal detection; a systematic uncertainty due to assumptions on the shape of the lateral distribution function; and an uncertainty due to shower-to-shower fluctuations [21]. The last term con-

tributes a factor of about 10%, while the contribution of the first two terms depends on energy and varies from 20% (at $S(1000) = 1.5$ VEM, equivalent to $\sim 0.3\,\mathrm{EeV}$) to 6% (at 200 VEM, equivalent to $\sim 40\,\mathrm{EeV}$).

The FD energy resolution is determined by propagating the statistical uncertainty on the light flux, the invisible energy uncertainty due to shower fluctuations and the uncertainties on EAS geometry and VAOD profiles. The overall energy resolution is 7.6% and it is almost constant with energy.

3 Energy Calibration

The analysis of the golden hybrid events leads to a relation between S_{38} and E_{FD}. The main challenge in this part of the analysis is to suppress the bias coming from the inclusion of events with energy below the trigger saturation threshold. The SD is fully efficient above energies of $3\,\mathrm{EeV}$ [16]. The upward fluctuations of $S(1000)$ below this energy would introduce a large bias in the energy conversion. In our past work [15], events below the threshold energy were rejected by a χ^2 method. As an evolution of this procedure, in the present study, a maximum likelihood (ML) method is used (see also [22]). This method, as the previous one, is based only on the data and does not depend on simulations. The ML function takes into account the evolution of uncertainties with energy, as well as event migrations due to the finite resolution of the SD. The ML method has been tested with the dataset used in the previous analysis and reproduces the same results as the χ^2 method: the ML method is mathematically more rigorous. The method has then been applied to the present sample of 839 selected hybrid events with energy $E_{\mathrm{FD}} \geq 3\,\mathrm{EeV}$ (see Section 2).

The relation between S_{38} and E_{FD} is well described by a single power-law function,

$$E_{\mathrm{FD}} = A\, S_{38}^{B}, \qquad (1)$$

where the resulting parameters from the data fit are $A = (1.68 \pm 0.05) \times 10^{17}\,\mathrm{eV}$ and $B = 1.035 \pm 0.009$. The most energetic selected event has an energy of about $75\,\mathrm{EeV}$.

The relative difference in the energy measured by the SD, $E_{\mathrm{SD}}(S_{38})$, using this energy calibration and the previous one [15] is tabulated in the second column of Table 1. The changes in the energy scale are due to an update of the absolute calibration of the FD pixels and improvements to the FD reconstruction, which now properly treat the lateral width of Cherenkov emission, multiple scattering of light, and the temperature and humidity dependence of quenching of fluorescence emission. Part of the difference between this energy calibration and the previous one is due to the introduction of the fiducial cuts. When not applying them, the energy changes by the factor reported in the third column of Table 1. The changes in calibration curves are smaller than the systematic uncertainty due to the application of the calibration method, of about 7% at $10\,\mathrm{EeV}$ and 15% at $100\,\mathrm{EeV}$ [15].

E_{FD}	$E_{\mathrm{new}}/E_{\mathrm{old}} - 1$	$E_{\mathrm{new}}/E_{\mathrm{nofid}} - 1$
$3\,\mathrm{EeV}$	$(+1.0 \pm 1.7)\%$	$(+0.4 \pm 1.6)\%$
$10\,\mathrm{EeV}$	$(-3.1 \pm 1.3)\%$	$(-1.3 \pm 1.7)\%$
$100\,\mathrm{EeV}$	$(-10 \pm 3)\%$	$(-4 \pm 4)\%$

Table 1: Relative differences in the new energy calibration, E_{new}, for different values of E_{FD}, with respect to the old calibration [15], E_{old}, (second column) and to the case when no fiducial cuts are applied in the event selection (E_{nofid}, third column).

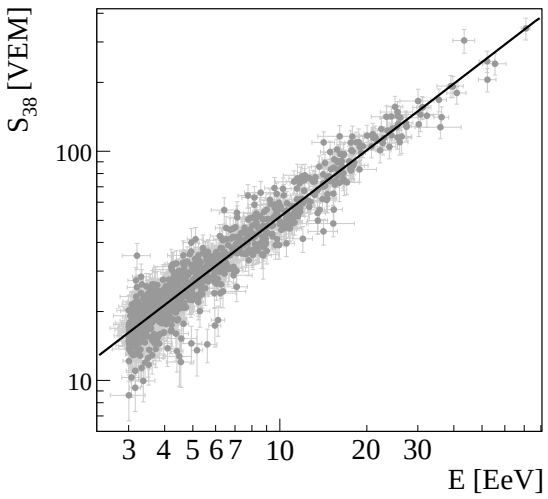

Figure 2: Correlation between S_{38} and E for the 839 selected hybrid events used in the fit. The most energetic event has an energy of about $75\,\mathrm{EeV}$.

The resolution in the SD energy, E_{SD}, can be inferred from the distribution of the ratio $E_{\mathrm{SD}}/E_{\mathrm{FD}}$ [23], fixing the FD energy resolution to the previously quoted 7.6%. The fit for three distinct ranges of energy is shown in Figure 3. The resulting SD energy resolution, with its statistical uncertainty, is $\sigma_E/E_{\mathrm{SD}} = (15.8 \pm 0.9)\%$ for $3\,\mathrm{EeV} < E_{\mathrm{SD}} < 6\,\mathrm{EeV}$, $\sigma_E/E_{\mathrm{SD}} = (13.0 \pm 1.0)\%$ for $6\,\mathrm{EeV} < E_{\mathrm{SD}} < 10\,\mathrm{EeV}$ and $\sigma_E/E_{\mathrm{SD}} = (12.0 \pm 1.0)\%$ for $E_{\mathrm{SD}} > 10\,\mathrm{EeV}$.

The total systematic uncertainty on the FD energy scale is about 22%. It includes contributions from the absolute fluorescence yield (14%) [10], calibration of the fluorescence telescopes (9.5%), the invisible energy correction (4%) [24], systematics in the reconstruction method used to calculate the shower longitudinal profile (10%), and atmospheric effects ($6\% \div 8\%$) [18]. The atmospheric uncertainties include those related to the measurements of aerosol optical depth ($5\% \div 7.5\%$), phase function (1%) and wavelength dependence (0.5%), the atmosphere variability (1%) [25] and the residual uncertainties on the estimation of pressure, temperature and humidity dependence of the fluorescence yield (1.5%).

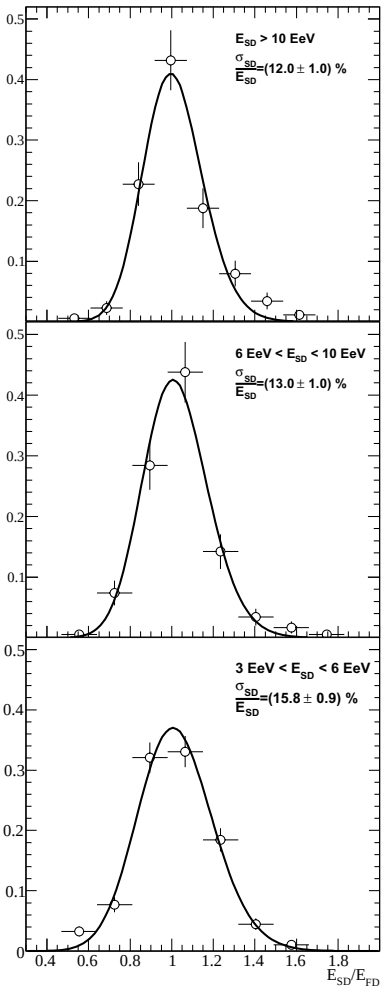

Figure 3: Ratio $E_{\rm SD}/E_{\rm FD}$ for the selected events for various ranges of energy. The lines represent the ratio distribution function for the data [23].

4 Conclusions

The energy calibration of the SD array of the Pierre Auger Observatory has been studied using a method based on the data only. It takes into account all the known systematic uncertainties and their dependencies on energy. In this analysis a new fiducial cut in the event selection is also introduced, in order to avoid systematic effects dependent upon the composition of the primary particles.

The results of this method are in good agreement with the previous studies of the energy calibration [15]. The differences are due to some improvements in the energy reconstruction and an update of the calibration constants of the fluorescence telescopes, as well as to the introduction of the new fiducial cut.

The energy spectrum derived from data of the SD array is calibrated using the method presented in this paper and combined with a spectrum based on hybrid data only in [26].

References

[1] The Pierre Auger Collaboration, Nucl. Instr. Meth. A, 2004, **523**: 50–95.
[2] T. Suomijarvi, for the Pierre Auger Collaboration, Proc. 31st ICRC, Łódź, Poland, 2009, arXiv:0906.2354 [astro-ph].
[3] F. Salamida, for the Pierre Auger Collaboration, Proc. 31st ICRC, Łódź, Poland, 2009, arXiv:0906.2189 [astro-ph].
[4] M. Risse and D. Heck, Astropart. Phys., 2004, **20**: 661–667.
[5] H. Barbosa *et al.*, Astropart. Phys., 2004, **22**: 159–166.
[6] A.M. Hillas, Acta Physica Academiae Scientiarum Hungaricae, 1970, **29**, suppl. 3: 355–360.
[7] D. Newton, J. Knapp and A.A. Watson, Astropart. Phys., 2007, **26**: 414–419.
[8] M. Unger *et al.*, Nucl. Instr. Meth. A, 2008, **588**: 433–441.
[9] K. Louedec, for the Pierre Auger Collaboration, paper 0568, these proceedings.
[10] M. Nagano *et al.*, Astropart. Phys., 2004, **22**: 235–248.
[11] M. Ave *et al.*, Astropart. Phys., 2007, **28**: 41–57; M. Ave *et al.*, Nucl. Instr. Meth., 2008, A **597**: 46–49.
[12] S. Ostapchenko, Proc. of the ISVHECRI (Pylos, Greece), 2004, **151**: 143–146, arXiv: hep-ph/0412332.
[13] A.G Mariazzi, for the Pierre Auger Collaboration, paper 0950, these proceedings.
[14] T. Pierog *et al.*, Czech. J. Phys., 2006, **56**: A161–A172.
[15] C. Di Giulio, for the Pierre Auger Collaboration, Proc. 31st ICRC, Łódź, Poland, 2009, arXiv:0906.2189 [astro-ph].
[16] The Pierre Auger Collaboration, Nucl. Instr. Meth., 2010, A **613**: 29–39.
[17] The Pierre Auger Collaboration, Phys. Lett. B, 2010, **685**: 239–246.
[18] The Pierre Auger Collaboration, Astropart. Phys., 2010, **33**: 108–129.
[19] The Pierre Auger Collaboration, Phys. Rev. Lett., 2010, **104**: 091101.
[20] J. Hersil et al., Phys. Rev. Lett., 1961, **6**: 22–23.
[21] M. Ave, for the Pierre Auger Collaboration, Proc. 30th ICRC, Merida, Mexico, 2007, **4**: 307–310, arXiv:0709.2125 [astro-ph] .
[22] H. Dembinski, for the Pierre Auger Collaboration, paper 0724, these proceedings.
[23] R.C. Geary, J. R. Stat. Soc., 1930, **93**: 442–446.
[24] The Pierre Auger Collaboration, Nucl. Instr. Meth. A, 2010, **620**: 227–251.
[25] M. Will, for the Pierre Auger Collaboration, paper 0339, these proceedings.
[26] F. Salamida, for the Pierre Auger Collaboration, paper 0893, these proceedings.